JOURNAL OF SOLID STATE CHEMISTRY 114, 6–14 (1995)

On the Iron Oxidation State in the Iron-Substituted γ Nickel Oxyhydroxides

L. Demourgues-Guerlou, L. Fournès, and C. Delmas[1]

Laboratoire de Chimie du Solide du CNRS and Ecole Nationale Supérieure de Chimie et Physique de Bordeaux, Université Bordeaux I, 351, cours de la Libération, 33405 Talence Cedex, France

Received September 7, 1993; in revised form March 2, 1994; accepted March 4, 1994

In order to improve the knowledge of the electrochemical cycling process that involves the hydrated iron-substituted nickel hydroxides, the cationic oxidation state distribution in γ-oxidized materials has been studied. Magnetic measurements and Mössbauer data show that, for small iron compositions, most of the iron ions are in the low-spin tetravalent state, while for higher iron concentrations, the Fe^{3+} (HS) ions are stabilized. Comparison with the homologous cobalt system suggests that the oxidation state of the substituting cation varies in order to accommodate the crystal field imposed by the prevailing cations. © 1995 Academic Press, Inc.

INTRODUCTION

Partial substitution of iron for nickel in the nickel hydroxides leads to the stabilization of the electrochemical cycling between the α- and γ-hydrated varieties, as shown previously (1, 2). The structures of both materials are schematically represented in Fig. 1. The α-reduced phase is stabilized by the electrostatic interactions between the ions within the slab and the carbonate ions inserted in the interslab space in order to compensate for the excess positive charge due to the trivalent state of the iron ions (1, 3). Moreover, a strong hydrogen bond network exists between the slab hydroxyls and the intercalated water molecules. In the γ-type phases, the $Ni_{1-y}Fe_yO_2$ slabs are linked by alkali cations inserted in the interslab space. The α/γ cycling is completely stabilized for the iron-substituted materials, due to the stability of the Fe^{3+} ions. However, the substitution of iron induces a noticeable increase in the cell voltage and, correlatively, a decrease in electrode chargeability, which limits the electrochemical performance for high iron amounts (2). To understand this behavior, which is strongly related to the high oxidizing character of the iron-substituted γ phases, the distribution of nickel and iron oxidation states in the materials must be determined. For this purpose, a characterization of the overall series of the iron-substituted γ phases ($0 \leq y \leq 0.50$) prepared by chimie douce has been performed from X-ray diffraction, magnetic measurements, and Mössbauer data, which are discussed in the present paper.

CRYSTAL CHEMISTRY

As reported in a previous paper, the iron-substituted γ phases are prepared by oxidizing hydrolysis, in (NaClO + KOH) medium, of the $NaNi_{1-y}Fe_yO_2$ ($0 \leq y \leq 0.7$) precursor phases (1). The formation of the γ phase, which exhibits the general formula

$$\underbrace{H_tNa_uK_w(H_2O)_z}_{\text{interslab space}}\ \underbrace{Ni_{1-y}Fe_yO_2}_{\text{slab}},$$

proceeds with the exchange of alkaline ions for protons and the intercalation of water molecules. While the nickel and iron ions are trivalent in the precursor phase, their average oxidation state is in the 3.34–3.66 range in the γ phases.

As shown in Fig. 2, the changes in the oxidation state and in the interslab space composition lead to strong modifications of the lattice parameters. The increase in the interslab distance during the oxidizing hydrolysis is due to the intercalation of water molecules and alkaline ions in the interslab space. Besides, the metal–metal intrasheet distance decreases during oxidation as expected from the ionic radii. In addition, the monoclinic distortion due to the Jahn–Teller effect of Ni^{III} (LS) ions that characterizes the $NaNi_{1-y}Fe_yO_2$ phase for $0 \leq y < 0.20$ is not observed for the γ phases whatever the value of y. This behavior suggests the existence of two oxidation states for nickel.

The metal–metal distance increases with increasing y, which results from the difference in ionic radius between the nickel and iron ions; whatever the oxidation state of both ions (+3 or +4), the iron ions are larger than the nickel ions (4).

A different effect had been noted in the case of the

[1] To whom correspondence should be addressed.

0022-4596/95 $6.00

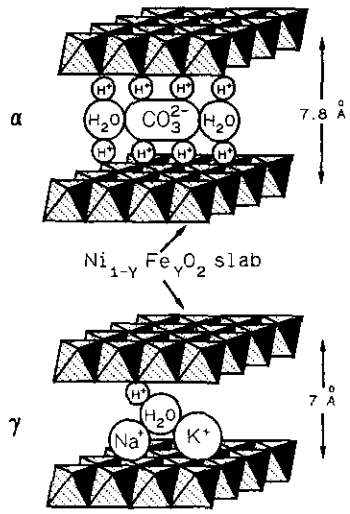

FIG. 1. Schematic structural representation of the iron-substituted α^* and γ phases.

substitution of cobalt for nickel. No significant modification in the a parameter was detected, whereas the values of the ionic radii imply a decrease (5). The fact that the value of the a parameter in the unsubstituted γ phase (2.82 Å) is close to the minimal distance between two O^{-2} ions ($r_{O^{-2}} = 1.40$ Å (4)) suggests that the lattice is virtually close packed in the plane, so that no contraction upon the substitution of cobalt for nickel is possible.

AVERAGE CATIONIC OXIDATION STATE

The average oxidation state of the nickel and iron ions within the slab in the γ phases has been determined by iodometric titration. The results are summarized in Table 1 for $0.10 \leq y \leq 0.50$. For the homologous cobalt-substituted materials, the values of the cationic oxidation state are close to 3.5 whatever the cobalt concentration (6, 7). In the case of iron substitution, the electrochemical study has given evidence of the strong oxidizing character of the oxyhydroxides, which is all the more pronounced as the iron concentration is higher (2). As a consequence, spontaneous partial reduction in air must occur and initiate a decrease in the oxidation state with increasing y, as shown in Table 1. This tendency to reduction is confirmed by a slow decrease with time of the average cationic oxidation state (determined by chemical titration) and especially of the iron oxidation state (evidenced by a ^{57}Fe Mössbauer spectroscopy study). Nevertheless, such a reduction occurs without any modification of the X-ray diffraction pattern of the material, even after several months of aging. However, in order to minimize the spontaneous reduction and to obtain comparable data for the various compositions, the magnetic and Mössbauer characterizations have been performed after short periods of aging.

TABLE 1
Average Oxidation State of the Transition Ions vs Iron Concentration in the γ Nickel Oxyhydroxides

	y					
	0.10	0.20	0.30	0.40	0.45	0.50
Oxidation state (±0.05)	*3.66*	*3.65*	*3.55*	*3.45*	*3.40*	*3.34*

MAGNETIC STUDY OF THE γ PHASES

Magnetic susceptibility measurements have been carried out with a DSM-8 susceptometer (MANICS) over

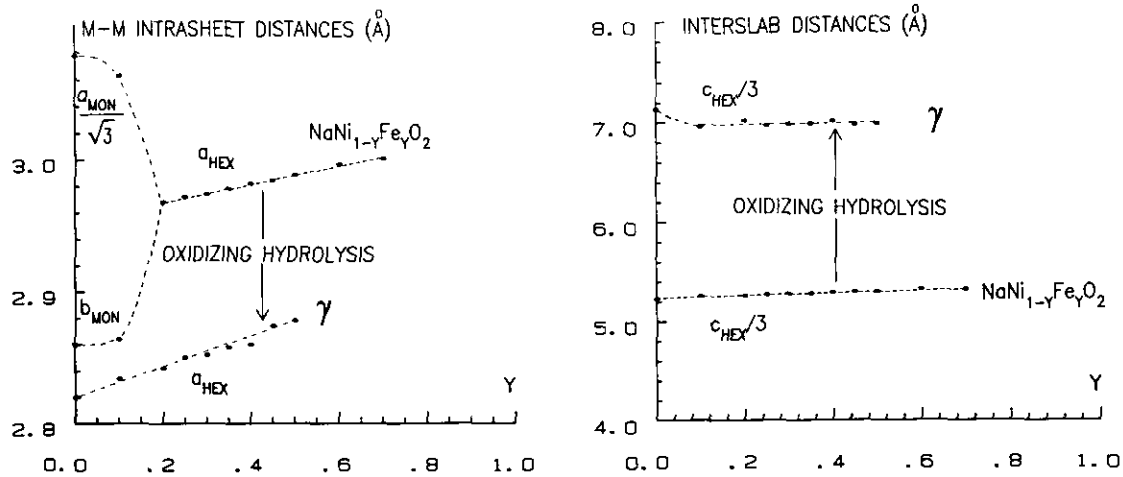

FIG. 2. Variation of the intrasheet and interslab distances during the oxidizing hydrolysis reaction from $NaNi_{1-y}Fe_yO_2$ precursor phases to γ phases.

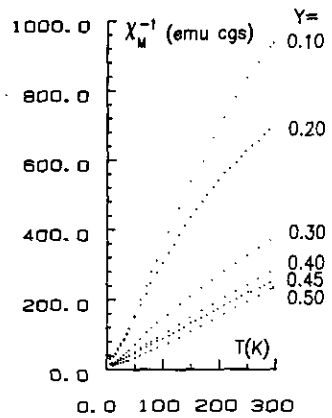

FIG. 3. Thermal variations of reciprocal molar magnetic susceptibilities for the iron-substituted γ oxyhydroxides ($0.10 \leq y \leq 0.50$).

the 4–300 K temperature range. The thermal variations of the χ_M^{-1} experimental reciprocal molar susceptibilities (corrected for diamagnetism) are given in Fig. 3 for various iron concentrations in the γ phases. The curve corresponding to the $y = 0.30$ composition is also reported with a more expanded scale in Fig. 4 (dotted line).

For $y \geq 0.45$, typical Curie–Weiss laws are observed while for lower iron concentrations, the curves exhibit a gradual variation of the slope vs temperature. The hypothesis of a TIP effect has been rejected as it would not lead to reasonable TIP values in this susceptibility range. In order to emphasize this behavior, for y values lower than 0.40, two Curie constants have been experimentally determined; the first is in the 30–100 K temperature range and the second is in the 200–300 K range. These values can be considered as the extreme observed values. Furthermore, taking into account the values of the average oxidation state of the nickel and iron ions (Table 1), the theoretical Curie constants have been calculated within the spin-only

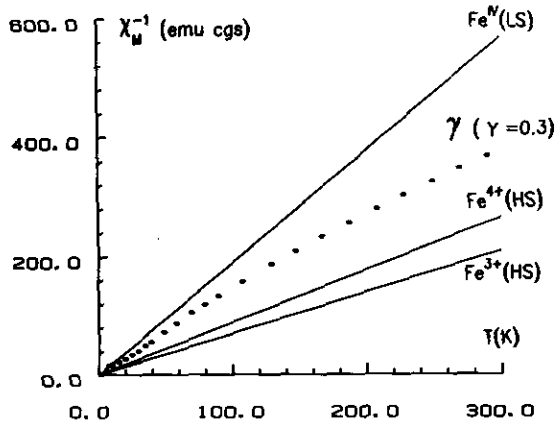

FIG. 4. Thermal variation of experimental and theoretical reciprocal molar magnetic susceptibilities for the γ ($y = 0.30$) phase.

TABLE 2
Comparison of the Experimental and Calculated Curie Constants for the Iron-substituted Oxyhydroxides ($0.10 \leq y \leq 0.50$)

		Curie constants		
			Experimental values	
y	Slab formula	Theoretical values	30–100 K Range	200–300 K Range
0.10	$Ni^{III}_{0.24}Ni^{IV}_{0.66}Fe^{3+}_{0.10}$ (HS)	0.53		
	$Ni^{III}_{0.34}Ni^{IV}_{0.56}Fe^{4+}_{0.10}$ (HS)	0.42	0.26	0.37
	$Ni^{III}_{0.34}Ni^{IV}_{0.56}Fe^{IV}_{0.10}$ (LS)	0.23		
0.20	$Ni^{III}_{0.15}Ni^{IV}_{0.65}Fe^{3+}_{0.20}$ (HS)	0.93		
	$Ni^{III}_{0.35}Ni^{IV}_{0.45}Fe^{4+}_{0.20}$ (HS)	0.73	0.32	0.62
	$Ni^{III}_{0.35}Ni^{IV}_{0.45}Fe^{IV}_{0.20}$ (LS)	0.33		
0.30	$Ni^{III}_{0.45}Ni^{IV}_{0.55}Fe^{3+}_{0.30}$ (HS)	1.37		
	$Ni^{III}_{0.45}Ni^{IV}_{0.25}Fe^{4+}_{0.30}$ (HS)	1.07	0.66	0.93
	$Ni^{III}_{0.45}Ni^{IV}_{0.25}Fe^{IV}_{0.30}$ (LS)	0.47		
0.40	$Ni^{III}_{0.15}Ni^{IV}_{0.45}Fe^{3+}_{0.40}$ (HS)	1.80		
	$Ni^{III}_{0.55}Ni^{IV}_{0.05}Fe^{4+}_{0.40}$ (HS)	1.40	0.99	1.10
	$Ni^{III}_{0.55}Ni^{IV}_{0.05}Fe^{IV}_{0.40}$ (LS)	0.60		
0.45	$Ni^{III}_{0.15}Ni^{IV}_{0.40}Fe^{3+}_{0.45}$ (HS)	2.02		
	$Ni^{III}_{0.55}Fe^{3+}_{0.05}$ (HS) $Fe^{4+}_{0.40}$ (HS)	1.90	1.18	
	$Ni^{III}_{0.55}Fe^{3+}_{0.05}$ (HS) $Fe^{IV}_{0.40}$ (LS)	0.82		
0.50	$Ni^{III}_{0.16}Ni^{IV}_{0.34}Fe^{3+}_{0.50}$ (HS)	2.25		
	$Ni^{III}_{0.55}Fe^{3+}_{0.16}$ (HS) $Fe^{4+}_{0.34}$ (HS)	1.82	1.47	
	$Ni^{III}_{0.50}Fe^{3+}_{0.16}$ (HS) $Fe^{IV}_{0.34}$ (LS)	1.23		

model according to three hypotheses about the oxidation state and spin configuration of the iron ions, with the nickel ions providing the overall charge compensation: (i) Fe^{3+} (HS), (ii) Fe^{4+} (HS), and (iii) Fe^{IV} (LS). The values of the experimental and theoretical Curie constants have been reported in Table 2, α for $0.10 \leq y \leq 0.50$. The theoretical thermal variations of reciprocal magnetic molar susceptibility (Curie law) corresponding to the previously mentioned hypotheses are also displayed in Fig. 4 with solid lines representing the $y = 0.30$ composition. Comparison of the experimental curves to the theoretical ones in Fig. 4, as well as comparison of the experimental Curie constants to the theoretical values in Table 2, shows unambiguously the presence of tetravalent iron ions and suggests that they are in the low spin configuration at low temperatures for $y \leq 0.40$. Therefore, the increase of the Curie constant with temperature may be attributed to a low spin → high spin transition of a fraction of the tetravalent iron ions.

^{57}Fe MÖSSBAUER SPECTROSCOPY STUDY

The Mössbauer spectra were recorded with a constant acceleration spectrometer using a room temperature ^{57}Co

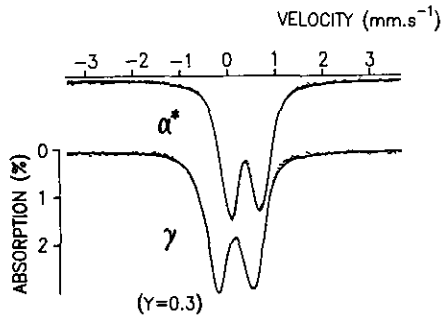

FIG. 5. Mössbauer spectra at room temperature of the α^* and γ phases for $y = 0.30$.

source (Rh matrix—activity 10 mCi) in a transmission geometry. The γ phase series ($0.10 \leq y \leq 0.50$) has been investigated at room temperature and the $y = 0.20$ and $y = 0.30$ compositions have been further studied in the 30–293 K temperature range with a variable temperature cryostat. As the results are quite similar in both cases, only the low temperature results concerning the $y = 0.30$ composition are presented in detail. All isomer shifts given in this paper refer to iron metal at room temperature.

Study of the γ ($y = 0.30$) Phase at Various Temperatures

The Mössbauer spectra of the γ (oxidized variety) and α^* (reduced variety) phases for $y = 0.30$ at room temperature are given in Fig. 5. As a result of the line broadening observed with regard to the instrumental width (~0.28 $mm \cdot s^{-1}$), the refinement of the Mössbauer parameters has been computed with a least-squares routine method using distributions of quadrupolar splittings. This means that, although all iron sites (and also nickel sites) that correspond to one distribution are identical from the structural point of view, they are different for Mössbauer spectroscopy since they are not exactly surrounded in the same way by nickel and iron ions as a result of the statistical distribution of these ions.

In the case of the α^* phase, the slight difference in intensity of the two lines may result from a textural effect due to a preferential orientation of the particles. This effect results from the fact that the nickel hydroxide particles are hexagonal-plate-shaped, as previously shown by transmission electron microscopy studies (7, 9). Moreover, the tendency to preferential orientation is emphasized on the X-ray diffraction spectra by the exalted intensity of the (00*l*) lines.

The spectrum of the α^* phase has been fitted to one distribution, the Mössbauer parameters of which ($\delta = 0.35$ $mm \cdot s^{-1}$, $\overline{\Delta} = 0.60$ $mm \cdot s^{-1}$) correspond as expected to Fe^{3+} (HS) ions (9).

The spectrum of the γ phase is shifted to lower velocity values, which suggests the presence of tetravalent iron ions in this material. Moreover, the difference in the width of the two lines leads one to fit the spectrum to the sum of two distributions, as reported in the following.

The behavior of the γ ($y = 0.30$) phase has been investigated at decreasing temperatures, to a lower limit of 30 K. The Mössbauer spectra, presented in Fig. 6, are strongly modified at decreasing temperatures; a broadening and a change in relative intensity of the two initial lines arise simultaneously. The Mössbauer parameters (δ_i, isomer shift, and $\overline{\Delta}_i$, average quadrupole splitting) of each distribution are summarized in Table 3 with the corresponding populations P_i, i.e., the molar ratio of the given iron population over the overall iron population. The values of the usual fit parameters MISFIT (which gives the fraction of the experimental signal that remains unfitted) and χ^2 (which represents the adequacy between the experimental and calculated data) have also been reported in Table 3. The low MISFIT values on one hand and the χ^2 values close to 1 on the other hand show good agreement between the experimental and calculated data. On the basis of the results reported in Table 3, the evolution of the populations assigned to the various components is depicted in Fig. 7.

At room temperature, the first distribution (P_1) is characterized by a δ isomer shift equal to 0.05 $mm \cdot s^{-1}$. This value has to be compared with those reported by several authors for trivalent and tetravalent iron ions:

* In K_2NiF_4 type structure materials such as $SrFeO_{2.75}$

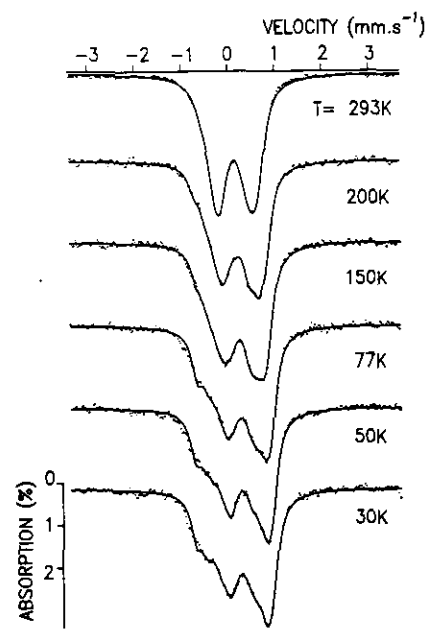

FIG. 6. Evolution of the Mössbauer spectra of the γ ($y = 0.30$) phase at decreasing temperature.

TABLE 3

Mössbauer Parameters (δ_i Isomer Shifts and $\bar{\Delta}_i$ Average Quadrupole Splittings) and Corresponding Populations Obtained for a γ ($y = 0.30$) Phase at Various Temperatures

	Fe^{IV} (LS)			$Fe^{(3.5+)}$			Fe^{3+} (HS)				
T (K)	δ_1 (mm·s^{-1})	$\bar{\Delta}_1$ (mm·s^{-1})	P_1	δ_2 (mm·s^{-1})	$\bar{\Delta}_2$ (mm·s^{-1})	P_2	δ_3 (mm·s^{-1})	$\bar{\Delta}_3$ (mm·s^{-1})	P_3	MISFIT	χ^2
293	0.05	0.88	0.22	0.15	0.70	0.78				0.01	0.95
200	0.06	0.99	0.25	0.15	0.78	0.52	0.40	0.59	0.23	0.07	0.63
150	0.05	1.00	0.25	0.18	0.81	0.50	0.40	0.52	0.25	0.04	0.80
77	0.10	1.14	0.31	0.20	0.98	0.41	0.42	0.56	0.28	0.03	0.85
	Fe^{IV} in site 1			Fe^{IV} in site 2							
	δ_1	$\bar{\Delta}_1$	P_1	δ_1'	$\bar{\Delta}_1'$	P_1'					
50	0.01	1.10	0.25	0.12	0.98	0.34	0.45	0.71	0.41	0.02	0.92
30	0.01	1.10	0.28	0.12	0.98	0.31	0.45	0.72	0.41	0.02	0.93

or $SrFeO_{3-x}F_{1-x}$, the isomer shift values reported for Fe^{3+}(HS) ions are 0.40 and 0.42 mm·s^{-1}, respectively (10, 11).

* The δ values observed for Fe^{4+}(HS) ions in various oxides with the general formula $(A, A')_2M_{0.50}Fe_{0.50}O_4$ (A = La, Sr, Ba; A' = La; M = Li, Mg, Zn, Ga, Ni) range from -0.20 to -0.14 mm·s^{-1} (12).

* The experimental δ value obtained for the γ phase ($\delta = 0.05$ mm·s^{-1}) is close to the values claimed by several authors for Fe^{IV} (LS) ions: from -0.04 to 0.00 mm·s^{-1} (12, 13, 14).

According to Parish, the range covered by the δ values for Fe^{IV} (LS) ions must be from +0.1 to +0.2 mm·s^{-1} (15). These values have been determined on the basis of theoretical calculations involving the difference in total electron density at the nucleus between the absorber and the standard. The difficulty in evaluating this parameter in a given material accounts for the difference between the theoretical δ values claimed by Parish and the experimental ones.

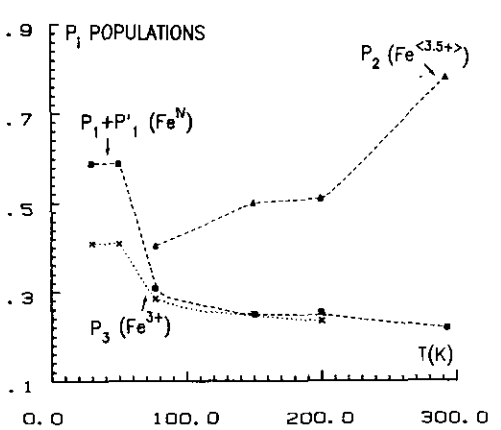

FIG. 7. Thermal evolution of the various iron populations observed by Mössbauer spectroscopy for the $y = 0.30$ composition.

These overall data lead us to assign the P_1 population in the γ phase to Fe^{IV} (LS) ions. Moreover, the existence of tetravalent iron ions in such a configuration is in good agreement with the magnetic study as well as with the evolution of the interatomic distances of the γ phases vs iron amount, as will be discussed in the penultimate section of the present paper.

As far as the second distribution (P_2) is concerned, the value of the average isomer shift (0.15), intermediate between those of Fe^{3+} (HS) and Fe^{IV} ions, suggests the presence of an average valence "$Fe^{(3.5+)}$" resulting from fast electron hopping between trivalent and tetravalent iron ions. A similar behavior involving Fe^{3+} (HS) and Fe^{4+} (HS) ions has already been reported in the case of $SrFeO_{2.75}$ and $SrFeO_{2.83}$ (10).

At decreasing temperatures to 77 K, the population of $Fe^{(3.5+)}$ intermediate valency iron (P_2) decreases; conversely, the population of Fe^{IV} ions increases and a third component (P_3) arises due to Fe^{3+} (HS) ions, as emphasized in Fig. 7. This behavior results from the decrease of the probability of Fe^{3+}–Fe^{4+} electron hopping at decreasing temperature. Below 50 K, the average valence iron distribution completely vanishes: the calculation gives evidence of one distribution of Fe^{3+} (HS) ions (P_3) and two distributions of Fe^{IV} (LS) ions (P_1 and P_1') exhibiting different Mössbauer parameters, as indicated in Table 3.

Provided that the "$Fe^{(3.5+)}$" distribution contains 50% trivalent iron ions and 50% tetravalent iron ions, the overall tetravalent iron population is equal to 0.61 at room

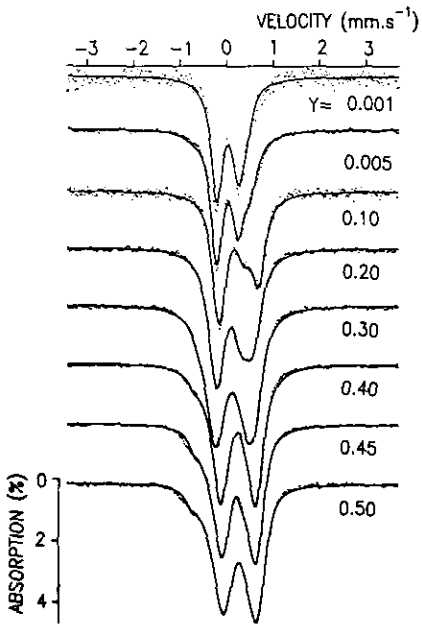

FIG. 8. Evolution with iron concentration of the room temperature Mössbauer spectra of the γ oxyhydroxides ($0.001 \leq y \leq 0.50$).

temperature. This value is very close to that calculated at 30 K by adding both Fe^{IV} distributions ($P_1 + P_1'$), i.e., 0.59.

For a given distribution, the increase in the isomer shift with decreasing temperature (observed for δ_1 and δ_2 between 293 and 77 K and for δ_3 between 200 and 30 K) must be noted. This effect, well known in Mössbauer spectroscopy, results from the contribution involving the second-order Doppler effect (9).

The investigation of the $y = 0.20$ composition has shown behavior quite similar to that reported above for $y = 0.30$, with a value of the overall tetravalent iron population equal to 0.68 at 40 K.

Study at Room Temperature of the γ Phases as a Function of Iron Concentration ($0.001 \leq y \leq 0.50$)

The spectra of the γ phases at room temperature are reported in Fig. 8. The $y = 0.001$ and $y = 0.005$ compositions were prepared with the ^{57}Fe isotope. Though these materials do not exhibit any interest from the electrochemical cycling viewpoint, they have been investigated so as to confirm the general evolution of the Mössbauer parameters.

This series of spectra shows a shift to higher velocity values with y increasing, as well as a strong change in the relative intensity of the two lines. This behavior gives evidence of a modification of the iron oxidation state vs y. As previously discussed for the γ ($y = 0.30$) phase, the spectra have been fitted to the sum of two distributions. The Mössbauer parameters and the P_i iron populations corresponding to each distribution have been summarized in Table 4. The MISFIT and χ^2 values, also reported in this table, show good agreement between the experimental and calculated data.

Whatever y, the first distribution isomer shift (δ_1) has to be attributed to Fe^{IV} (LS) ions, as previously observed for the $y = 0.30$ composition. As far as the other population is concerned, the isomer shift values correspond for $y \leq 0.40$ to $Fe^{(3.5+)}$ average valence ions (δ_2) and for higher concentrations to Fe^{3+} (HS) ions (δ_3).

The overall populations of trivalent iron ($P_{\text{tri Fe}}$ = (trivalent iron)/(overall iron) molar ratio) and tetravalent iron ($P_{\text{tetra Fe}}$ = (tetravalent iron)/(overall iron) molar ratio) have been calculated provided that the population of average valence iron ions P_2 contains 50% tetravalent iron and 50% trivalent iron;

$$P_{\text{tetra Fe}} = P_1 + P_2/2;$$

$$P_{\text{tri Fe}} = P_2/2 + P_3;$$

with $P_3 = 0$ for $y \leq 0.40$ and $P_2 = 0$ for $y > 0.40$

On the basis of the data given in Table 4, the evolutions of the populations assigned to iron distributions (P_1, P_2, P_3) have been displayed in Fig. 9 as a function of iron content. The variations of $P_{\text{tri Fe}}$ and $P_{\text{tetra Fe}}$ are also reported in this figure. For $y \leq 0.40$, the strong decrease with increasing y of the P_1/P_2 ratio induces a decrease of the tetravalent iron population and conversely an increase of the trivalent iron population. This evolution is strongly enhanced for $y = 0.45$, on account of the disappearance of the component assigned to $Fe^{(3.5+)}$ ions in favor of that of Fe^{3+} ions.

DISCUSSION

Evolution of the Iron Oxidation State vs y

In order to schematize the cationic distribution in the iron substituted γ oxyhydroxides, the variations of the tetravalent nickel population ($P_{\text{tetra Ni}}$ = (tetravalent nickel)/(overall nickel) molar ratio) and tetravalent iron population have been displayed in Fig. 10. The $P_{\text{tetra Ni}}$ values have been calculated from the $P_{\text{tetra Fe}}$ values reported in Fig. 9 and from the values of average cationic oxidation state summarized in Table 1. The variation of the overall concentration of tetravalent ions, i.e., the number of tetravalent ions (nickel or iron) per metal ion (N_{IV}), which is directly related to the average cationic oxidation state in the material, has also been displayed in Fig. 10.

Below $y = 0.40$, the gradual decrease with increasing y of both $P_{\text{tetra Fe}}$ and $P_{\text{tetra Ni}}$ populations results from the variation of the average cationic oxidation state (Table 1).

TABLE 4

Evolution with Iron Concentration (y) of the Mössbauer Parameters and of the Populations Corresponding to the Various Distributions Observed

	Fe^{IV} (LS)			Average Valency $Fe^{(3.5+)}$			Fe^{3+} (HS)				
y	δ_1 (mm·s^{-1})	$\bar{\Delta}_1$ (mm·s^{-1})	P_1	δ_2 (mm·s^{-1})	$\bar{\Delta}_2$ (mm·s^{-1})	P_2	δ_3 (mm·s^{-1})	$\bar{\Delta}_3$ (mm·s^{-1})	P_3	MISFIT	χ^2
0.001	0.01	0.47	0.80	0.20	0.67	0.20				0.38	1.17
0.005	0.01	0.50	0.62	0.15	0.66	0.38				0.17	2.11
0.10	0.12	0.48	0.37	0.25	0.85	0.63				0.01	0.99
0.20	0.05	0.58	0.34	0.18	0.72	0.66				0.01	0.99
0.30	0.05	0.88	0.22	0.15	0.70	0.78				0.01	0.95
0.40	0.02	0.91	0.19	0.25	0.72	0.81				0.08	2.99
0.45	0.06	0.90	0.39				0.30	0.69	0.61	0.07	2.60
0.50	0.01	0.96	0.25				0.30	0.69	0.75	0.05	2.07

Beyond $y = 0.40$, the decrease of the $P_{\text{tetra Fe}}$ population induces an increase of the Ni^{IV} population in order to perform the overall charge balance.

The variation of the oxidation state of the iron ions in the γ oxyhydroxides may be correlated to the evolution of the metal–metal intrasheet distances shown in Fig. 11. The amount of Fe^{3+} ions, deduced from the Mössbauer study at room temperature has also been reported vs y in this figure. It appears that both variations are strongly correlated. For $y \geq 0.45$, the Fe^{3+} (HS) amount increases rapidly; the larger size of these ions with regard to those of the Ni^{III} and Ni^{IV} ions induces a strong increase in the metal–metal intrasheet distance.

Comparison with the Homologous Cobalt System

The cationic distribution is quite the opposite in the homologous cobalt-substituted γ phase (6, 7): indeed, the cobalt ions remain trivalent for $y < 0.4$ (which induces the presence of Ni^{IV} ions); a very small number of Co^{IV} ions are detected only for higher y values. If the cationic distribution exclusively depended on the intrinsic stability of cobalt and iron ions, the opposite effect would be expected. Hence the cationic distribution of oxidation states and spin configuration that is actually stabilized must be that leading to the minimal internal elastic strains in the material, i.e., to the lowest energy system. In other words, the size of the substituting cation tends to be as close as possible to that of the prevailing nickel ion.

Indeed, when starting from the unsubstituted γ phase (0.50 Ni^{III} (d^7 LS)–0.50 Ni^{IV} (d^6 LS)), the substitution of Co^{III} (d^6 LS) to Ni^{III} (d^7 LS) ions is much more likely than that of Co^{IV} (d^5 LS) to Ni^{III} ions on account of the size of these ions ($r_{Co}III_{(LS)} = 0.53$ Å, $r_{Ni}III_{(LS)} = 0.56$ Å) (4).

In the case of iron substitution, let us assume that these ions would be Fe^{3+} (HS) ones, therefore exhibiting a large ionic radius ($r_{Fe^{3+}(HS)} = 0.63$ Å). In order to ensure the

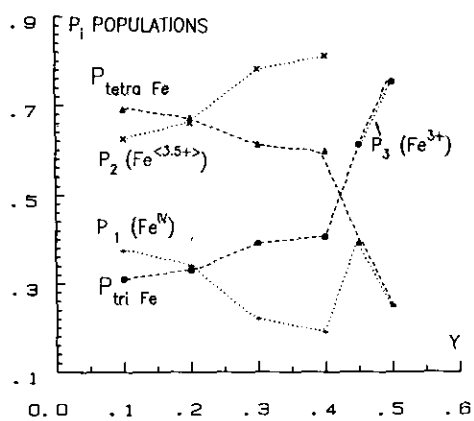

FIG. 9. Evolution with iron concentration of the P_1 (Fe^{IV}), P_2 ($Fe^{(3.5+)}$), P_3 (Fe^{3+}) iron populations and of the overall populations of trivalent iron ($P_{\text{tri Fe}}$) and tetravalent iron ($P_{\text{tetra Fe}}$).

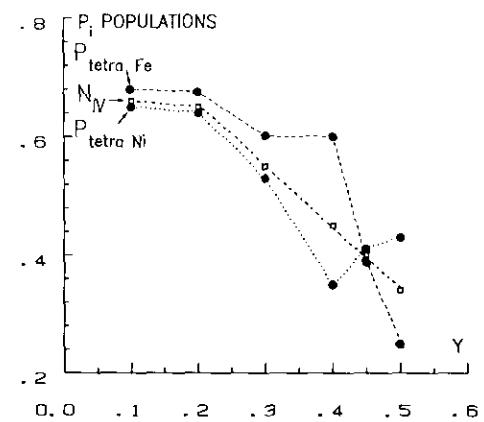

FIG. 10. Evolution with iron concentration of the population of tetravalent iron ($P_{\text{tetra Fe}}$) and tetravalent nickel ($P_{\text{tetra Ni}}$) in comparison with the overall concentration of tetravalent ions (N_{IV}).

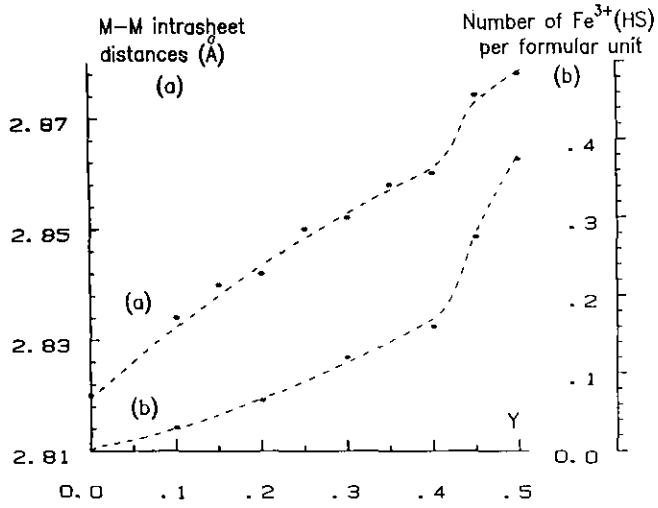

FIG. 11. Comparison of the variations vs y of the metal–metal intrasheet distance (a) and of the Fe^{3+} (HS) concentration (b) in the γ oxyhydroxides.

overall charge balance (average cationic oxidation state equal to 3.5), the main part of the nickel ions would consequently become tetravalent, so that the strong difference in size between Ni^{IV} and Fe^{3+} ions would entail excessive strain within the material. Hence, the opposite situation arises: so as to reduce the iron–oxygen distances, the iron ions stay mainly in the tetravalent state in the low spin configuration. In other words, the metal–oxygen distance is imposed by the prevailing cation within the slab.

Actually, for very small iron amounts, as a result of the strong ligand field induced by the nickel ions, the majority of the iron ions are in the tetravalent state in the low spin configuration. For the opposite case, for higher iron amounts, this average ligand field decreases, leading therefore to a decrease of the Fe^{IV} (LS) amount.

Evolution of the Iron Distribution vs y

On the basis of these general considerations, the variation vs y of the iron distribution determined by Mössbauer spectroscopy is discussed in the following. Provided that the iron ions are statistically distributed in substitution for $Ni^{3+/4+}$ ions in a triangular lattice, the existence of different iron environments has to be assumed:

(i) "Isolated" iron ions, i.e., surrounded by 6 nickel ions, are subject to a strong ligand field and will therefore be stabilized in the low spin tetravalent state.

(ii) Large clusters of iron ions, in which the ligand field is imposed by the iron ions themselves, will rather lead to the stabilization of Fe^{3+} (HS) ions.

(iii) Small clusters of iron ions, in which the ligand field is intermediate between those corresponding to both previous cases, will entail the presence of tetravalent iron ions mainly in the low spin configuration at low temperatures and in the high spin configuration at higher temperatures. Moreover, in this situation, Fe^{4+} (HS) and Fe^{3+} (HS) ions coexist, since Mössbauer spectroscopy shows an intermediate valence state $Fe^{(3.5+)}$, which is due to fast electronic hopping between Fe^{4+} and Fe^{3+} ions.

For very iron-diluted solutions, the (i) case is mainly observed (Table 4). Nevertheless, even for very small iron concentrations, a significant number of trivalent iron ions are present (10% and 19% for $y = 0.001$ and 0.005, respectively). Provided that the ions are isolated one from each other and not liable to interact, a probability calculation allows one to obtain the theoretical percentage of iron ions surrounded by 6 nickel ions: 99.4% and 97% for $y = 0.001$ and 0.005, respectively. These values are much larger than the real amounts of Fe^{IV} (LS) ions which gives evidence of the tendency to iron cluster formation in the real material.

When the iron amount increases, the number of small clusters (case (iii)) increases at the expense of the isolated iron ions.

For the highest iron amounts ($y \geq 0.45$), large clusters of Fe^{3+} ions are observed.

In the case of intermediate iron amounts ($0.10 \leq y \leq 0.40$), both isolated iron ions and small clusters are present. At decreasing temperature, the Fe^{3+}–Fe^{4+} hopping is frozen and a Fe^{4+} (HS) $\rightarrow$ Fe^{IV} (LS) ions transition occurs. It follows that two environment types appear for the Fe^{IV} (LS) ions: the isolated ones and those that belong to the small clusters. This is fully consistent with the existence of two Mössbauer distributions experimentally observed at low temperature for the Fe^{IV} (LS) ions (Table 3).

In conclusion, this work has shown that, for small iron substitution amounts, the iron ions are mainly in the low spin tetravalent state within the γ-type nickel oxyhydroxide. This result accounts for the very oxidizing character of this material tested in an electrochemical cell. Further Mössbauer and X-ray diffraction *in situ* studies in an electrochemical cell are now in progress.

ACKNOWLEDGMENT

The authors are grateful to C. Denage for technical assistance.

REFERENCES

1. L. Demourgues-Guerlou, J. J. Braconnier, and C. Delmas, *J. Solid State Chem.*, **104**, 359 (1993).
2. L. Demourgues-Guerlou and C. Delmas, *J. Electrochem. Soc.* **161**(3), 713 (1994).
3. L. Demourgues-Guerlou and C. Delmas, *J. Power Sources* **45**, 281 (1993).
4. R. D. Shannon and C. T. Prewitt, *Acta Crystallogr. B* **25**, 925 (1969).
5. C. Delmas, J. J. Braconnier, Y. Borthomieu, and P. Hagenmuller, *Mater. Res. Bull.* **22**, 741 (1987).

6. Y. Borthomieu, Thesis, University of Bordeaux I, 1990.
7. C. Faure, Thesis, University of Bordeaux I, 1990.
8. A. Delahaye, Thesis, University of Picardie, Amiens, France, 1986.
9. N. N. Greenwood and T. C. Gibb, "Mössbauer Spectroscopy." Chapman & Hall, London, 1971.
10. L. Fournès, Y. Potin, J. C. Grenier, G. Demazeau, and M. Pouchard, *Solid State Commun.* **62,** 239 (1987).
11. F. Menil, N. Kinomura, L. Fournès, J. Portier, and P. Hagenmuller, *Phys. Status Solidi A* **64,** 261 (1981).
12. L. Fournès, G. Demazeau, L. M. Zhu, N. Chevreau, and M. Pouchard, *Hyperfine Interact.* **53,** 335 (1990).
13. P. K. Gallagher, J. B. Mac Chesnay, and D. N. E. Buchanan, *J. Chem. Phys.* **41,** 2429 (1964).
14. M. Takano, N. Nakanishi, Y. Takeda, S. Naka, and T. Takeda, *Mater. Res. Bull.* **12,** 923 (1977).
15. R. V. Parish, "Mössbauer Spectroscopy" (D. P. E. Dickson and F. J. Berry, Eds.), Cambridge Univ. Press, London/New York, 1986.